JOURNAL OF GEOPHYSICAL RESEARCH, VOL. 92, NO. C13, PAGES 14,335–14,346, DECEMBER 15, 1987

The Equatorial Source of Propagating Variability Along the Peru Coast During the 1982–1983 El Niño

DAVID B. ENFIELD,[1] MARIA DEL PILAR CORNEJO-RODRIGUEZ,[2] ROBERT L. SMITH, AND PRISCILLA A. NEWBERGER

College of Oceanography, Oregon State University, Corvallis

Using data obtained from tide gages in South America, current meters along the equator and the Peru coast, and an array of pressure gages and inverted echo sounders within and around the Galapagos archipelago, we have analyzed the equatorial origin of coastal trapped waves observed by Cornejo-Rodriquez and Enfield (this issue) along the Peru coast during the intense 1982–1983 El Niño. The propagating fluctuations along the coast were much stronger at that time than either before or after the El Niño, and the variability was not locally forced by coastal winds. We find that the coastal variability was also more energetic during previous El Niño occurrences. At periods of 1–2 weeks the meridional component of currents on the equator is up to an order of magnitude more energetic than the zonal fluctuations and is consistently associated with sea level that fluctuates antisymmetrically between hemispheres. At periods longer than 2 weeks the zonal velocity component is more energetic, and the cross-equatorial sea level variability is symmetric. The meridional and zonal phase structures of cross spectra involving the currents and sea level establish the 1- to 2-week equatorial fluctuations as mixed Rossby-gravity (Yanai) waves of low wave number with infinite phase speed (standing oscillations) in the middle of the band (10 days); the corresponding structures for longer periods are consistent with nondispersive Kelvin waves. Frequency domain EOF modes of the sea level and current data establish the mixed Rossby-gravity waves as the principal source of the strong trapped wave variability in the 1- to 2-week band along the Ecuador-Peru coast during the 1982–1983 El Niño episode.

1. INTRODUCTION

Poleward propagating fluctuations with periods in the 1- to 2-week band have been detected in sea level along the Peru coast during the El Niño events of 1976–1977 and 1982–1983 [*Smith*, 1978; *Brink et al.*, 1978; *Romea and Smith*, 1983; *Cornejo-Rodriguez and Enfield*, this issue]. The variability is incoherent with the coastal winds and has characteristics consistent with those of freely propagating, first baroclinic mode coastal trapped waves [*Brink*, 1982]. The objective of this study is to answer a question that has perplexed oceanographers for some time: Do these fluctuations originate in the equatorial waveguide? If so, what is the dominant form of equatorial variability that gives rise to them?

Kelvin waves are the most frequently observed long waves on the equator, and their dominance at low frequencies (periods of a few weeks or more) seems to account (at least partially) for the remarkable simulation capabilities of relatively simple numerical modeling schemes [e.g., *Busalacchi and O'Brien*, 1980, 1981]. *Wyrtki* [1975] describes El Niño–Southern Oscillation (ENSO) events as the result of equatorial Kelvin waves generated by major wind relaxations in the western and central Pacific. *Knox and Halpern* [1982] document a low-frequency pulse in equatorial sea level and currents with the characteristics of equatorial Kelvin waves. Using lagged cross-correlation analysis of band-passed (1–180 days) island sea levels, *Lukas et al.* [1984] detect zonal propagation along the equator that is consistent with low-frequency Kelvin waves. *Eriksen et al.* [1983] examine sea level fluctuations in the 1- to 6-week period band during 1978–1980 at equatorial Pacific islands and find evidence of wind-generated Kelvin waves traveling across the Pacific.

Attempts to identify equatorial Kelvin waves as the source of the coastal variability have not been very successful, however. *Romea and Smith* [1983] have analyzed the 1976–1977 currents and sea level fluctuations in the 0.1- to 0.2-d^{-1} (cpd) frequency band along the Peru coast (5°–15°). They found poleward propagating fluctuations with phase speeds of 2–3 m/s which were incoherent with the local coastal winds. They tried to establish a link between the coastal fluctuations in the days–weeks band and equatorial variability by comparing one tide station in the Galapagos Islands (Baltra Island, 27 km south of the equator) with the stations along the Peru coast. They could find only tenuous evidence to support equatorially trapped Kelvin waves as the source of the coastal propagating signals.

Cornejo-Rodriguez and Enfield [this issue] have analyzed sea level and wind series from stations in the eastern equatorial Pacific for the 1979–1984 period. During the 1982–1983 ENSO, they found a dramatic increase in sea level energy levels in the 8- to 11-day band at coastal stations (Figure 1) but not at Santa Cruz (near the equator). They show that the strong, poleward propagating coastal signals in the 8- to 11-day band were superimposed on a weaker, locally forced variability. They also note that the weakness of the signal in the 8- to 11-day band at Santa Cruz is consistent with the antisymmetric meridional structure of sea surface displacement in equatorially trapped, mixed Rossby-gravity (MRG) waves. Consistent with this, the weak connection found by *Romea and Smith* [1983] between Baltra sea level and the coast suggests that antisymmetric (off-equatorial, MRG) variability may dominate over symmetric (near-equatorial, Kelvin) fluctuations at these frequencies. No other free waves are predicted in this band by the theory of equatorial waves.

[1] Now at NOAA Atlantic Oceanographic and Meteorological Laboratory, Miami, Florida.
[2] Now at Facultad de Ingenieria Maritima y Ciencias del Mar, Escuela Politecnica del Litoral, Guayaquil, Ecuador.

Paper number 7C0686.
0148-0227/87/007C-0686$05.00

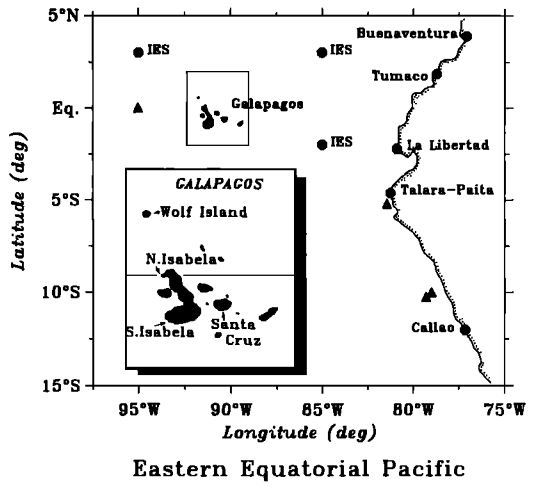

Fig. 1. Circles indicate the locations of coastal tide gage stations and oceanic inverted echo sounders (IESs); triangles show the positions of current meter moorings. (Inset) Locations of the Santa Cruz tide gage and the three pressure-temperature gages in the Galapagos archipelago.

There have been relatively few observations of MRG waves at the ocean surface, but *Wunsch and Gill* [1976] argue that such waves can be excited in the 9- to 10-day period band under large zonal scale (low wave number) wind forcing. *Luther* [1980] finds some evidence to support this possibility from the cross spectra of sea level between zonally separated, near-equatorial islands. Antisymmetric sea level variability that is consistent with such waves has also been detected. Thus *Ripa and Hayes* [1981] recognize the presence of both Kelvin and MRG waves in the first and second empirical orthogonal function (EOF) modes of a cross-equatorial array of subsurface pressure gages within the Galapagos archipelago. Also, *Chiswell et al.* [1987] have studied the meridional and zonal phase structures in sea level inferred from inverted echosounders deployed in the eastern equatorial Pacific during the 1982–1983 ENSO episode. They show that antisymmetric variability at periods of 6–10 days had the characteristics of lowest baroclinic mode MRG waves. *Clarke* [1983] has argued that the coastal variability in the 5- to 25-day period band may be due primarily to incident MRG waves, but was unable to confirm this because simultaneous equatorial and coastal data sets were not available.

We have used data from coastal and equatorial stations (Figure 1) to extract both the Kelvin and MRG components of equatorial variability and to compare them with the propagating response along the coast. We use the very distinct amplitude, phase, and propagation structures of Kelvin and MRG waves to separate the two wave forms in our data and determine the relative importance of these wave types. Following a discussion of the theoretical characteristics of equatorial waves (section 2) and description of the data (sections 3 and 4), we apply spectral analysis to the time series of sea level during the 1982–1983 ENSO episode (section 5). After showing the consistency between the sea level and current data (section 6), we synthesize the analyses with frequency domain empirical orthogonal functions (FDEOFs) (section 7). All of our data, equatorial and coastal currents included, are consistent with the dominance of MRG waves in the 1- to 2-week band along the equator and demonstrate their strong connection with the trapped coastal fluctuations.

2. EQUATORIAL WAVES

The governing equations for equatorial long waves were first developed by Laplace for shallow water on a rotating sphere. Their solution consists of an infinite set of meridional modes that obey the dispersion relation $(\omega/c)^2 - k^2 - \beta k/\omega = (2n + 1)\beta/c$, where ω is frequency, k is wave number, c is a separation constant (also the gravity wave speed), f is the Coriolis parameter, $\beta = df/dy$, and y is the meridional coordinate [*Moore*, 1968; *Moore and Philander*, 1977; *Gill*, 1982]. The integer n is the order of the Hermite polynomial that governs each of the modes.

The dispersion curves for a subset of the modes are plotted in Figure 2 as a function of dimensionless frequency and wave number. The slope of a line connecting the origin with points (ω, k) on a curve gives the phase velocity of the corresponding wave; the slope of the tangent to the curve at the same point gives its group velocity. For positive (negative) wave numbers the phase propagation is toward the east (west). There are four classes of waves: the Kelvin wave ($n = -1$), inertia-gravity waves ($\beta k/\omega$ small, $n \geq 1$, high frequencies), Rossby waves (ω^2/c^2 small, $n \geq 1$, low frequencies), and the mixed Rossby-gravity wave, or Yanai wave ($n = 0$). Phase propagates eastward for the Kelvin wave and westward for Rossby modes, while inertia-gravity and MRG waves may propagate in either sense. Energy propagates eastward for Kelvin and MRG waves but in either sense for inertia-gravity and Rossby waves. The dispersion relation for the MRG wave is

$$\omega/c - k - \beta/\omega = 0 \tag{1}$$

The name for this wave arises from the fact that its dispersion curve approaches that of the short ($n = 1$) Rossby wave at large negative wave numbers and that of the Kelvin (gravity) wave at large positive wave numbers.

There is a range of frequencies with upper and lower bounds at ω_u and ω_l within which neither inertia-gravity nor Rossby waves can exist (Figure 2). The corresponding range of wave periods for a typical separation constant of 2.5–3.0 m/s

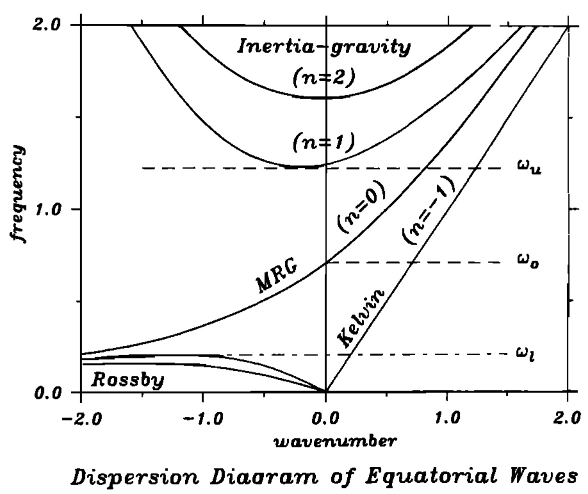

Fig. 2. Theoretical dispersion curves for a subset of equatorial waves. The vertical axis is the nondimensional frequency ω^* (scale factor $(2\beta c)^{1/2}$), and the horizontal axis is the nondimensional wave number (scale factor $(2\beta/c)^{1/2}$), where $c = 2.5$ m/s. The reflectionless gap is defined by the upper and lower bounds $\omega^* = 1.22$ and $\omega^* = 0.20$, and the MRG crossover occurs at $\omega^* = 0.70$ (see discussion in the text).

(first baroclinic mode) extends from 5–6 days to 30–33 days. Hence wave energy in the 1- to 4-week period range can only propagate eastward in the form of Kelvin and MRG waves. When it impinges on an eastern boundary, the energy cannot be reflected in the form of inertia-gravity waves or long Rossby waves and must continue poleward along the coast as trapped waves [*Clarke*, 1983].

Equatorial Kelvin waves propagate eastward nondispersively with water particle velocities that are everywhere parallel to the equator. The sea surface displacement is maximum at the equator and falls off symmetrically to the north and south with a Gaussian shape (Figure 3). For the typical stratification found in the equatorial Pacific, the gravity wave speed is in the range 2.5–3.0 m/s, and the meridional decay scale (equatorial radius of deformation) is several hundred kilometers. The MRG wave has an antisymmetric displacement profile with extrema near $\pm 3°$ to $\pm 4°$ and no displacement at the equator (Figure 3). Particle velocities are entirely meridional at the equator, but both components are nonzero off the equator. Note that the MRG dispersion curve (Figure 2) crosses the zero wave number axis where $\omega^2 = \omega_0{}^2 = \beta c$. For a typical value of $c = 2.5$ m/s this occurs at a period of $T_0 = 9.6$ days, which we call the "MRG crossover." The crossover is special because the phase speed goes through a discontinuity there, being negative (positive) to the left (right) of the frequency axis. At the crossover itself, there is a superposition of two waves of infinite wavelength and phase speed, one traveling east, the other west (Figure 4). This yields a standing wave of infinite wavelength (the energy, however, propagates eastward).

In Figure 4 we show the Kelvin and MRG phase spectra for two hypothetical sea level stations located near the equator with a zonal separation of 1000 km, assuming a separation constant $c = 2.5$ m/s. Calculated values of the phase lie between $\pm 180°$, so that physical phases differing by multiples of 360° are indistinguishable. We refer to this as "phase wrapping." Thus the phase relationship for (nondispersive) Kelvin waves consists of a set of parallel straight lines that phase-wrap away from the origin with positive slope. The phase spectrum of MRG waves is very different from that of Kelvin waves. The MRG waves are highly dispersive, traveling westward ($T > T_0$) or eastward ($T < T_0$), or not at all when they consist of standing oscillations near $T = T_0$.

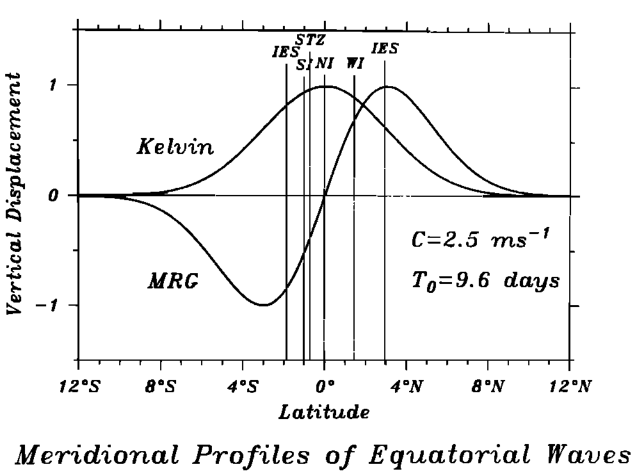

Fig. 3. Meridional surface displacement profiles for lowest vertical mode equatorial Kelvin and MRG waves. The sea level displacement is computed for a separation constant $c = 2.5$ m/s. The vertical lines indicate the meridional locations of stations shown in Figure 1 (abbreviations are defined in Table 1).

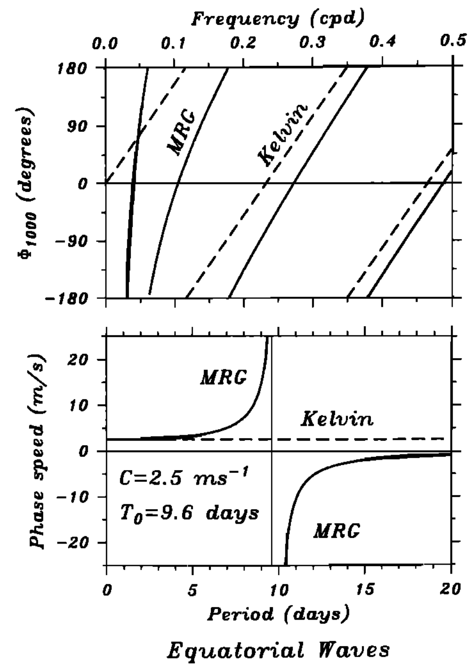

Fig. 4. (Top) Phase spectra for MRG (solid curves) and Kelvin (dashed curves) waves traveling between two sea level stations located near the equator with a zonal separation of 1000 km. Note that for frequencies at the MRG crossover ($f_0 \approx 0.1$ cpd), MRG waves are in phase due to their large phase speeds, while Kelvin waves are out of phase. (Bottom) Phase speed as a function of the period.

At the eastern boundary the incident energy must continue poleward into both hemispheres as coastal trapped waves. Poleward of the the equatorial deformation radius for the incident waves the coastal wave variability will have characteristics of free waves that do not depend on the nature of the equatorial waves from which they arise. The coastal waves are hybrid; they depend on both the topography of the continental margin and the density structure in the water column. At sufficiently low latitudes (equatorward of 15°S on the Peru coast) both theory and observations indicate that they behave much like internal Kelvin waves trapped by a vertical boundary, because the offshore scale of the waves is typically larger than the scale of the coastal topography [*Allen and Romea*, 1980; *Brink*, 1982].

3. DATA

Several types of data (Table 1) were used for this analysis: sea level height (SLH) from tide gages (TGs) in Colombia, Ecuador, and Peru, dynamic height from inverted echo sounders (IESs) deployed in an array around the Galapagos Islands, subsurface pressure from pressure-temperature gages (PTGs) deployed within the Galapagos archipelago, and current meters located along the equator at 95°W and 110°W and over the continental shelf and slope along the Peru coast at 5°S and 10°S. All data used are from within the 1982–1983 ENSO event, September 1982 through November 1983.

The station locations for the data are shown in Figure 1. We used data from five mainland TGs and one near the equator in the Galapagos: Buenaventura, Tumaco, La Libertad,

TABLE 1. Station Locations and Sources for Sea Level Height (SLH) and Current Meter (CM) Mooring Data

SLH Station	Abbreviation	Latitude	Longitude	Source
Echo sounder	IES	3°00′N	95°00′W	URI
Echo sounder	IES	3°00′N	85°00′W	URI
Echo sounder	IES	2°00′S	85°00′W	URI
Wolf Island	WI	1°24′N	91°50′W	PMEL
North Isabela	NI	0°03′S	91°28′W	PMEL
Santa Cruz	STZ	0°45′S	90°18′W	UH
South Isabela	SI	0°59′S	91°30′W	PMEL
Buenaventura	BVA	3°54′N	77°05′W	IGAC
Tumaco	TCO	1°50′N	78°44′W	IGAC
La Libertad	LLB	2°12′S	80°55′W	INOCAR
Talara	TPA	4°37′S	81°17′W	DHNM
Paita	TPA	5°05′S	81°07′W	EPOCS
Callao	CAL	12°03′S	77°09′W	DHNM

CM Mooring	Latitude	Longitude	Source
95°W equator	0°02′N	95°03′W	PMEL
110°W equator	0°03′N	109°10′W	PMEL
5°S shelf	5°06′S	81°21′W	OSU
10°S shelf	10°04′S	78°59′W	OSU
10°S slope	10°13′S	79°20′W	OSU

Data sources are University of Hawaii (UH), Instituto Oceanografico de la Armada del Ecuador (INOCAR), Direccion de Hidrografia y Navegacion de la Marina del Peru (DHNM), the Instituto Geografico Agustin Codazzi de Colombia (IGAC), The National Oceanic and Atmospheric Administration's Equatorial Pacific Climate Studies (EPOCS) program, University of Rhode Island (URI), Pacific Marine Environmental Laboratory (PMEL), and Oregon State University (OSU).

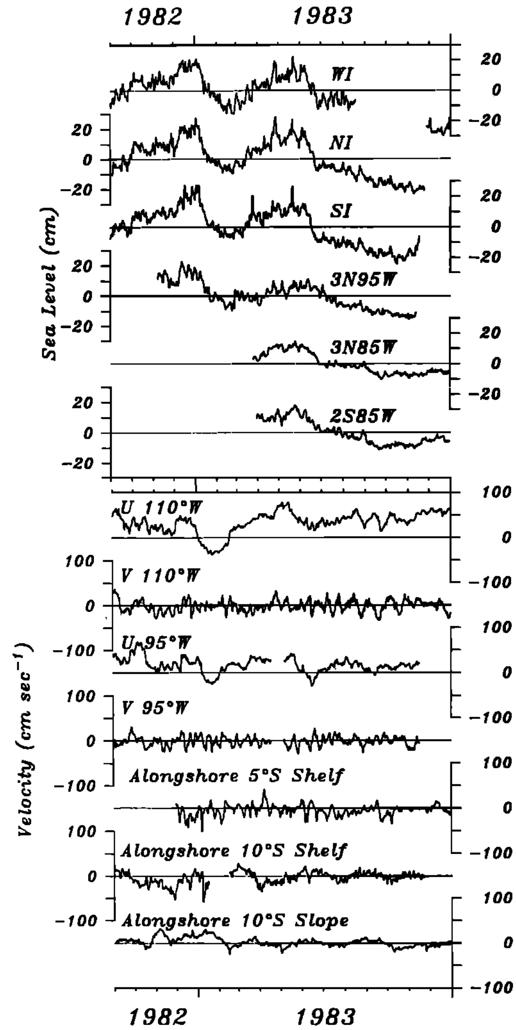

Fig. 5. (Top) Time series of sea level at echo sounders and pressure gages in the Galapagos. Geographic lcoations are shown in Figure 1, and abbreviations are defined in Table 1. (Bottom) Time series of currents at equatorial and coastal locations shown in Figure 1 and Table 1.

Talara-Paita, Callao, and Santa Cruz. The hourly TG data were checked for errors and corrected, then small gaps (2–3 days or less) in the series were filled using an autoregressive filter [*Anderson*, 1974] or by regression on nearby stations not used in the analyses. The 1982–1984 data from a tide gage at Paita (5°S) installed under the National Oceanic and Atmospheric Administration's Equatorial Pacific Ocean Climate Studies (EPOCS) program was spliced by regression to the 1979–1981 data from Talara (less than 50 km to the north), which subsequently deteriorated badly in quality and continuity. We refer to the combined series as Talara-Paita, although for the period of this study, all the data are from the Paita gage.

To suppress the influence of the diurnal and semidiurnal tides, the sea level series were low-pass (LLP) filtered using a cosine-Lanczos filter with a half-amplitude near 40 hours and then decimated to obtain 12 hourly series. The time coverage of the LLP data is shown in Figure 5 for the PTGs, IESs, and current meters. The time series of coastal SLH (except Tumaco) can be seen in Figure 2 of *Cornejo-Rodriguez and Enfield* [this issue], but the availability of coastal data was not critical in the design of our analysis. For some of our analyses it was necessary to remove very long time scale variability in sea level (especially the large-amplitude shifts during El Niño). Hence the LLP series were further smoothed using a very low pass (VLP) filter with a half-amplitude near 30 days, and the VLP series were subtracted from the LLP series.

The PTGs were deployed under the EPOCS program at three island locations in the Galapagos: Wolf Island, North Isabela, and South Isabela (data provided courtesy S. Hayes, Pacific Marine Environmental Laboratory (PMEL)). Four IES gages were deployed in the eastern Pacific in a box array around the Galapagos as part of EPOCS. The IESs at 3°N, 95°W; 3°N, 85°W; and 2°S, 85°W yielded useful records; the data were kindly provided by M. Wimbush (University of Rhode Island) in dynamic meters, and we converted them to centimeters of sea level. The interpretation of the IES data in terms of dynamic height and their sensitivity to salinity variations and modal structure are discussed by *Chiswell et al.* [1986]. Both the PTG and IES data have been processed and filtered by the data providers in manners analogous to our own TG data [see *Ripa and Hayes*, 1981; *Chiswell et al.*, 1987].

Current meter data from the EPOCS moorings at 95°W and 110°W were obtained from PMEL courtesy of D. Halpern. These data sets and those from the Peru shelf moorings at 5°S and 10°S and slope mooring at 10°S were filtered with the same LLP filter as the sea level. None of the moorings had current meters below 400 m, precluding any analysis of vertical modal structures, and some of the time series had gaps, so

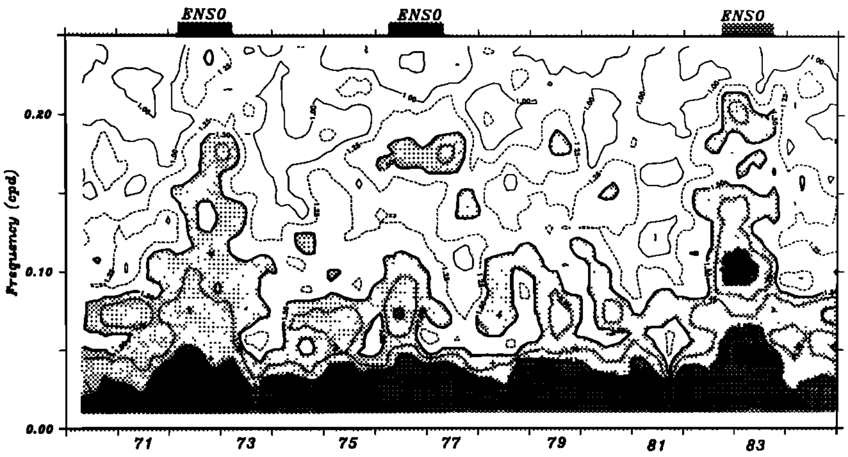

Fig. 6. Contour plot of the log of spectral density (cm^2/d) as a function of time and frequency for the sea level at Callao. The chance probability that a feature lies more than 0.26 above a given value is less than 10%. Dark (light) shading indicates log values above 2.0 (1.5). Contour interval is 0.25.

depth-averaged currents were calculated. To form this average, the data from each meter are weighted by the amount of the water column that they represent, and this transport is divided by the depth sampled (250 m for 95°W and 110°W; 100 m for 5°S and 10°S shelf; 350 m for 10°S slope). If all of the meters on the mooring were operating, the weighted average of the data is used. If one or more of the series is missing, an objective estimate of the average is made from the existing series and the cross correlations among the series [*Chelton et al.*, 1982]. Current meter data were used for the period from May 9 to November 7, 1983. During this period the data coverage is excellent. At 95°W one of the seven meters did not function for the last 2 weeks of the period. At 110°W, no estimation was necessary. Approximately 2 months of data were missing from the deepest of the four current meters on the 10°S slope mooring, while at each of the shelf moorings, one of the two meters was missing for much of the last month. The time period used is contained within a single mooring period at all locations, except at 110°W, where a gap of less than 3 days was bridged. We use only the alongshore component of the Peru coastal currents.

4. Enhanced Variability During El Niño Events

Before proceeding further, we wish to emphasize the special character of the 1- to 2-week fluctuations in Peru coastal sea level found by *Cornejo-Rodriguez and Enfield* [this issue]. They show that this variability was about an order of magnitude more energetic during the 1982–1983 El Niño episode than before or after that event. Remotely forced, propagating fluctuations can be clearly identified in 1982–1983 and are consistent with unforced coastal trapped waves, similar to those that have been documented by others for the 1976–1977 time period, also considered an El Niño. Only weak evidence for such propagating variability could be found for the intervening (non-ENSO) years, suggesting a unique association with El Niño conditions. To put our 1982–1983 observations in historical perspective, we will now show that enhanced sea level variability is indeed a characteristic feature along the Peru coast during ENSO occurrences.

We have processed 15 years of hourly sea level from Callao for the 1970–1984 period, which includes three known ENSO episodes: 1972–1973, 1976–1977, and 1982–1983. The intensities of these episodes have been classified by *Quinn et al.* [this issue] as strong, moderate, and very strong, respectively. To determine the distribution of energy with time as well as frequency, autospectra have been computed for the LLP series for successive 250-day data segments centered at 50-day intervals with a 200-day overlap between segments. The spectra are smoothed by applying a running band average with 10 degrees of freedom (d.f.), and the log of the spectral density is contoured in Figure 6.

A nearly 10-fold increase in the Callao SLH variance occurs in the 1- to 2-week band during 1982–1983, just as *Cornejo-Rodriguez and Enfield* [this issue] observed at Talara-Paita (their Figure 7). In addition, Figure 6 also shows an increase over a wide range of frequencies during the 1972–1973 ENSO event, classified as a strong event by *Quinn et al.* [this issue]. The earlier increase was similar to but not as intense as during the 1982–1983 ENSO (a centenary event by most estimates). A third increase occurred during 1976–1977, but this period is the least spectacular of the three and is mainly restricted to lower frequencies. Hence the energy increase in coastal SLH variability is a characteristic feature of ENSO episodes and occurs roughly in proportion to the overall intensity of the ENSO anomalies.

In this paper we concentrate our analysis exclusively on data acquired during the 1982–1983 ENSO occurrence, when the high-frequency (>0.07 cpd) coastal variability was especially intense and clearly propagating as coastal trapped waves. Our ability to demonstrate the existence and type of connection between the coastal variability and equatorial waves depends critically on measurements of equatorial currents and off-equatorial sea level. The latter, in particular, are only available for the 1982–1983 ENSO episode from the IES deployments. The lack of near-equatorial information from current meters or IESs during the 1970s precludes an analysis of the previous ENSO events.

5. Antisymmetric Versus Symmetric Variability

We begin our analysis by testing the simple hypothesis that antisymmetric SLH variability in the 1- to 2-week period range is the dominant waveform along the equator and between hemispheres along the coast. We have done this in two ways: by making cross-equatorial comparisons of phase and by looking for zonal propagation phase signatures of equatorial Kelvin and MRG waves.

5.1. *Meridional Comparisons*

A straightforward consequence of MRG dominance is that coastal sea level variability on either side of the equator will be out of phase. As a test for this condition, we calculated cross spectra between stations that lie 2°–5° off the equator (on opposite sides). Sea level is compared between Buenaventura and Talara-Paita and between Tumaco and La Libertad for the period from September 1982 to September 1983, and between the IESs at 85°W for April through September 1983. We smoothed the spectra with a running band average on eight successive frequencies, with five overlapping frequencies, obtaining 16 d.f. per band and a bandwidth of 0.02 cpd (Figure 7).

In general, the coherence (γ) is frequently high and significant at frequencies less than 0.222 cpd (4.5 days). Most of the γ^2 values in the 7- to 11-day band are significant above the 90% confidence level. The coherence at higher frequencies is generally low and seldom significant. For the 0.020- to 0.080-cpd frequency range (periods greater than 12.5 days), the phase fluctuates around zero, suggesting the presence of Kelvin wave variability. For the 0.096- to 0.149-cpd frequency range (6.7–10.4 days) the phases are distributed near $\pm 180°$ or are large and positive, suggesting an antisymmetric relation consistent with the dominance of MRG waves. A qualitatively similar cross spectrum is found for the Tumaco-Libertad comparison.

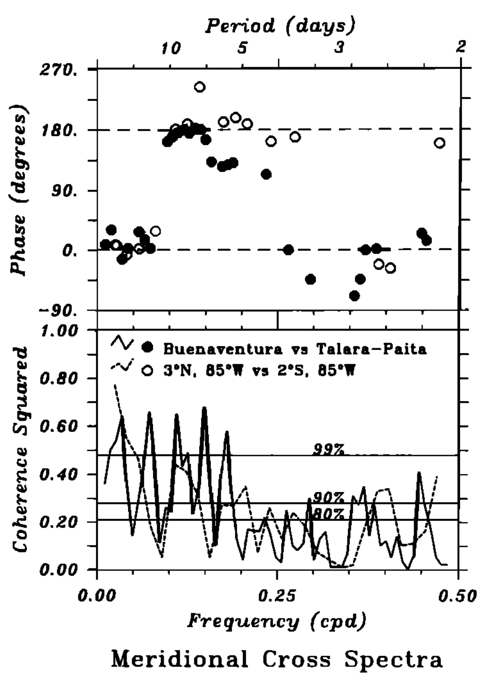

Fig. 7. Sea level cross spectra between Buenaventura and Talara-Paita and between the echo sounders at 85°W. (Top) Phase estimates plotted for coherence-squared (γ^2) values at the 80% confidence level or higher. Northern hemisphere lags southern hemisphere for positive phase. (Bottom) The γ^2 spectra with the significance levels shown for various degrees of statistical confidence.

We have also computed the cross spectra between Buenaventura and Talara SLH series for periods before (June 1981 to June 1982) and after (December 1983 to May 1984) the 1982–1983 ENSO event. We do not find evidence in the coherences or phases for antisymmetric variability during these non-ENSO intervals; coherences are generally much lower in the 1- to 2-week band, and phases are either indeterminate (pre-ENSO) or favor the presence of symmetric variability (post-ENSO). In summary, the cross-equatorial phase relationships, both at the coast and on the equator, are consistent with the dominance of Kelvin waves at periods of 2 weeks or more, and of MRG waves at periods of 6–11 days, but the latter only during the 1982–1983 ENSO episode.

5.2. *Zonal Propagation Signatures*

To investigate wave propagation structures, we have also computed the cross spectra between zonally separated sea level stations in the equatorial zone, including the near-equatorial coastal station, La Libertad. In particular, we are looking for phase spectra that reproduce the phase distributions expected for Kelvin and MRG waves (Figure 4). With eight stations to choose from, we can compute a number of cross spectra for zonal separations of several hundred kilometers or more. Moreover, to take advantage of the distinct behaviors of MRG and Kelvin waves, we have also computed cross spectra where one of the series consists of the sum or difference of the IESs at 85°W and the other series from a single station (IES at 3°N, 95°W; TG/PTGs in the Galapagos; La Libertad). The effect of meridional differences in variance at 85°W is reduced by normalizing the band-passed (LLP-VLP) series with their rms values. The presumption is that antisymmetric (symmetric) variability is enhanced by the differences (sums) of the normalized series and suppressed by the sums (differences). All cross spectra are computed for the period from April 21 to October 21, 1983.

A representative subset of the cross spectra is shown in Figure 8, with the theoretical curves (Figure 4) superimposed on the phase spectra for a gravity wave speed of 2.4 m/s. This speed is representative of the least squares fits summarized in Table 2 and discussed below. The spectra fall into two groups that are readily rationalized in terms of the sum/difference argument or the expected amplitudes of symmetric versus antisymmetric variability with distance from the equator (Figure 3). Cases involving the summed series and/or stations close to the equator (Galapagos) have significant coherence primarily at the low frequencies and phase distributions that (where coherent) are reasonable for Kelvin waves. With difference series and/or stations away from the equator the coherence is significant in the 1- to 2-week band, and phases lie along the appropriate distribution for MRG waves. Computations involving the IES at 2°S, 85°W also show high coherence at higher frequencies. The phases in both the symmetric and antisymmetric groups are consistent with curves based on the same gravity wave speed (separation constant), as one expects.

A particular result is that phases for the antisymmetric group consistently cluster around zero near the 10-day period, and the crossover period inferred from the fitted line is $T_0 =$ 9.8 days. In other words, the MRG dominance is concentrated in a frequency range for which zonal phase speeds are very large, i.e., the variability consists essentially of standing oscillations. However, when coherent variability extends to the higher frequencies, the MRG variability propagates eastward more slowly (yet faster than Kelvin waves), as expected.

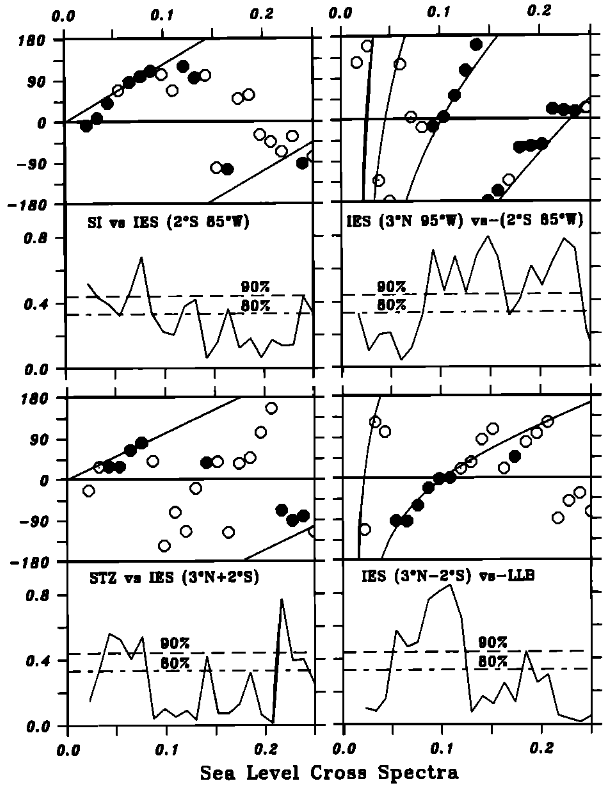

Fig. 8. (Left) Phase and coherence spectra for selected pairs of zonally separated, near-equatorial sea level time series. Upper panels show spectra between individual stations; lower panels are for summed or differenced series at 85°W versus data at stations to the east or west. Data in the left (right) panels are shown with the theoretical dispersion curves for Kelvin (MRG) waves superimposed (c = 2.4 m/s). Station abbreviations are defined in Table 1.

For each cross spectrum the phase distribution was examined to see if the phases fall clearly along the propagation characteristic for one of the two possible wave types, Kelvin or MRG (Figure 4, upper panel). Such was the case except where Wolf Island was concerned, which has very low coherence with other stations and uninterpretable phases. The phase spectra were fitted by least squares to the corresponding theoretical curves (lowest vertical mode) using phase estimates for which the coherence is significant at the 80% confidence level or higher. The fit statistics are shown in Table 2 (upper group).

TABLE 2. Least Squares Fits to Phase Data for Zonally Separated Station Pairs

Station Pair	Fit Type	R^2	Frequency Range	Speed, m/s	Period, days
			SLH-SLH		
3°N/85°W-Libertad	MRG	0.98	0.093–0.126	2.7	9.3
2°S/85°W-Libertad	MRG	0.95	0.087–0.153	2.2	10.2
3°N/95°W-2°S/85°W	MRG	0.99	0.093–0.280	2.2	10.3
3°N/95°W-3°N/85°W	MRG	0.99	0.098–0.230	2.3	10.0
2°S/85°W-North Isabela	Kelvin	0.93	0.016–0.082	2.9	8.9
2°S/85°W-Santa Cruz	Kelvin	0.96	0.016–0.082	3.3	8.3
2°S/85°W-South Isabela	Kelvin	0.95	0.016–0.087	2.6	9.4
Dif.85°W-Libertad	MRG	0.99	0.087–0.190	2.9	8.9
Dif.85°W-3°N/95°W	MRG	0.96	0.087–0.245	2.0	10.7
			Current-SLH		
E-W, 95°W-2°S/85°W	Kelvin	0.99	0.016–0.240	2.3	10.0
N-S, 95°W-2°S/85°W	MRG	0.99	0.087–0.230	2.2	10.1
N-S, 95°W-3°N/85°W	MRG	0.99	0.066–0.224	2.4	9.8

The westernmost station is listed first in each instance. Except as noted in the text, the frequency range used depends on the distribution of coherence squared estimates at the 80% significance level or higher (the criterion for using a phase estimate). For both wave types the fitted parameter is the gravity wave speed, or separation constant (c) for the family of equatorial waves to which the fitted curves belong. The MRG crossover period is $T_0 = 2\pi(\beta c)^{-1/2}$. The R^2 statistic is the coefficient of determination.

Kelvinlike distributions were fitted to a straight line constrained to pass through the origin; only frequencies below 0.1 cpd were considered, where the spectra were coherent and the phases meaningful. The slope of the fitted line is the estimated gravity wave speed (Kelvin phase speed) over the frequency range for which coherent estimates were available (periods greater than 10 days). It is also the estimated separation constant (c) for the family of dispersion curves to which the fitted line belongs.

The MRG-like phase distributions were fitted to the theoretical hyperbolic function derived from (1):

$$\phi = (L_x/c)\omega - (\beta L_x)\omega^{-1} \tag{2}$$

where ϕ is the phase (radians) and L_x is the station separation. Because the MRG fits are very sensitive to errors at low frequencies and low-frequency phases were often ambiguous, the fits were done only for frequencies above 0.085 cpd. (Because of the generally low coherence of MRG-like distributions at low frequencies, few estimates were neglected.)

Although the estimates of c tend to be lower for MRG cases (2.4 m/s) than for Kelvin cases (2.7 m/s), they are not statistically different, and they all fall within a reasonable range for observed gravity wave speeds on the equator. Because small errors in phase result in large differences in c at low frequencies, and due to the smaller frequency ranges used, the Kelvin fits are less significant. The approximate 95% confidence intervals for c are (2.1, 3.8) and (2.2, 2.7) for the Kelvin and MRG fits, respectively. We therefore consider 2.4 m/s to be our best estimate of the gravity wave speed along the equator in the eastern Pacific during the 1982–1983 ENSO.

6. EQUATORIAL CURRENTS

Current meter measurements on the equator act as natural filters for the purpose of distinguishing between the presence of Kelvin versus MRG waves. At least three theoretical relationships involving the velocity components can be used in discriminating between the two wave types.

1. Flow dominance. On the equator, Kelvin waves are associated only with zonal flow (u) variability, and MRG waves only with meridional current (v).

2. Phase relationships at a single longitude. Sea level (ζ) and u are in phase for Kelvin waves at all frequencies, while sea level north (south) of the equator lags (leads) v by $\pi/2$ for MRG waves [*Gill*, 1982].

3. Zonal propagation. For Kelvin waves the phase spectra for zonally separated time series of u, ζ, or both should show phases distributed along a nondispersive gravity wave characteristic (Figure 4). For MRG waves, zonally separated series of v or ζ alone should give dispersive distributions of phase as shown in Figure 4, with zero phase at the crossover frequency. A v series versus a zonally separated ζ series north (south) of the equator should result in an MRG phase spectrum similar to either variable alone but shifted by $\pi/2$ in the sense of v leading (lagging) ζ.

We first examine relationship 1 through an autospectral analysis of zonal and meridional flow components at the

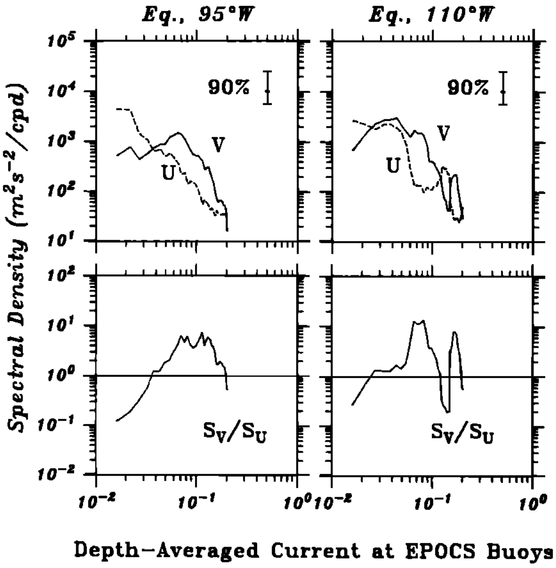

Fig. 9. (Top) Autospectra of the zonal and meridional components of depth-averaged current velocity at the 95°W and 110°W equatorial moorings. (Bottom) Ratios of the spectral coefficients of meridional velocity to those of zonal velocity.

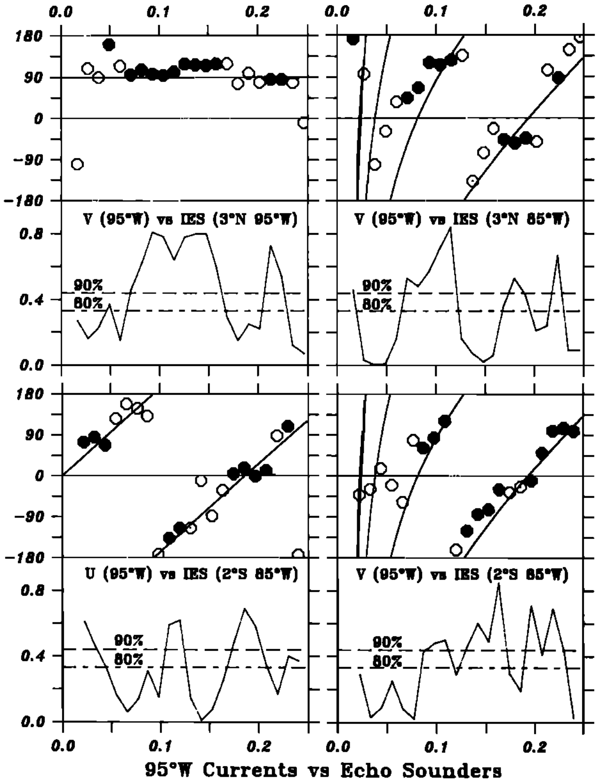

Fig. 10. Phase and coherence spectra for the zonal or meridional component of current velocity versus sea level at selected locations. The theoretical dispersion curves for Kelvin waves (lower left) and MRG waves (right panels) are superimposed on three of the phase spectra ($c = 2.4$ m/s).

EPOCS buoys. We then test for relationship 2 by calculating the cross spectrum between the 95°W current components and SLH at 3°N, 95°W. Finally, using relationship 3, we search for Kelvin (MRG) wave propagation by calculating the cross spectrum between u and v at the 95°W buoy and ζ at the 85°W IESs. We note that relationship 2 is also implicit in the $\pi/2$ offset between the phase spectrum of zonally separated v versus ζ and the corresponding spectrum for either variable alone (relationship 3).

All calculations shown in this section are done for the common data period from May 9 through November 7, 1983. The results are robust, however, because they are reproduced for other time periods for which there is data coverage.

6.1. *Flow Dominance*

The autospectra for zonal and meridional currents at both of the equatorial moorings are shown in Figure 9 along with the ratio of the spectral estimates for the two components (S_v/S_u). The spectra for u are very red, without large peaks, while the v spectra are much less red and show a relative maximum of energy in a frequency band corresponding to periods of 1–2 weeks. At the lowest frequencies the u component is most energetic, while the v energy prevails in the 1- to 2-week band and exceeds S_u by an order of magnitude. The same calculations done for a 230-day period starting in September 1982 (not shown) indicate similar structures except that the 1- to 2-week peak at 110°W is not as broad and the one at 95°W is centered near 0.10 cpd. Hence the energy distributions for currents are consistent with the preponderance of Kelvin waves at low frequencies, while MRG waves are the dominant form in the band around 10 days. These results confirm the similar conclusion suggested by cross-equatorial comparisons of sea level (section 5.1, Figure 7).

6.2. *Sea Level Versus Currents at 95°W*

Figure 10 shows the cross spectrum between the meridional velocity and SLH at 3°N, along 95°W. The coherence is quite strong in a wide band covering periods of 6–14 days. With only two exceptions, the phases are close to the $\pi/2$ offset expected for MRG waves, even when the coherence is low. This spectrum is impossible for other equatorial wave types, Kelvin waves in particular. It constitutes very strong support for the existence of MRG waves over a wide range of frequencies. The cross spectrum between zonal velocity and sea level at 3°N did not give meaningful results, probably because the Kelvin wave should have a small amplitude at this latitude.

6.3. *Phase Propagation*

The other three panels of Figure 10 show the coherence and phase spectra for the velocity components at 95°W versus sea level at the 85°W IESs. The spectrum for the zonal flow at 95°W versus sea level at 2°S, 85°W has coherent bands near periods of 100, 8–10, and 5–6 days and shows a very clear, nondispersive propagation consistent with Kelvin waves. For reference, we show the theoretical phase curves for a gravity wave speed of 2.4 m/s, although the least squares fit to the phases gave 2.3 m/s (Table 2). The corresponding spectrum for the IES at 3°N, 85°W (not shown) was less coherent and had only a wide, random scattering of phases that could not be interpreted in terms of any known wave type. Once again, Kelvin waves are preferentially "selected" by the zonal velocity on the equator, so the lack of signal at 3°N is most likely due to the rapid poleward decrease of the sea level amplitude for Kelvin waves beyond the equatorial radius of deformation.

The cross spectra for the meridional velocity are generally more coherent than for the zonal velocity, especially at periods of about 2 weeks or less. Their phases are also distributed in a regular fashion, but their orientation is not as linear as for the zonal flow and does not project toward zero phase at zero frequency. They lie, instead, along the theoretical phase curve for MRG waves having a separation constant about equal to the observed Kelvin wave speed. In particular, the meridional velocity leads sea level by $\pi/2$ (+90°) near the crossover frequency (0.10 cpd), as expected for MRG waves, and they are well distinguished from the expected Kelvin wave phases at that frequency.

We have also tried other combinations of current velocity and SLH from various sources (TGs and PTGs at the Galapagos), including the sums and differences of cross-equatorial SLH pairs. Most of these are considerably less coherent than the cases shown in Figure 10 and do not show a clear selection of wave types over wide frequency ranges within a single spectrum. However, coherent bands near the crossover period (10 days) are a robust feature and consistently have phases near +90° (merdional velocity leads/lags SLH in the northern/southern hemisphere). Not surprisingly, we repeatedly find that the use of velocity components is a more effective method for discriminating between wave types than are cross-equatorial sums and differences of sea level (section 5). Also, the IESs are more effective detectors of MRG variability than the island-based TGs and PTGs, probably due to their higher latitude and more favorable exposure.

Kelvin waves are, of course, deselected by the meridional velocity in favor of MRG waves, just as the zonal component selects in favor of Kelvin waves. The results shown in Figure 10 therefore demonstrate conclusively the coexistence of both equatorial wave types over a wide frequency range but do not show clearly which is the dominant form. Other evidence (Figures 7 and 9) shows that MRG waves consistently dominate in the 1- to 2-week period band, while Kelvin waves are preponderant at lower frequencies.

7. FREQUENCY DOMAIN EOF ANALYSIS

To obtain an integrated overview of the data sets in the 1- to 2-week frequency band, we performed two FDEOF analyses, one on the sea levels and the other on the currents. The use of FDEOFs was introduced in meteorological applications by *Wallace and Dickenson* [1972] and *Wallace* [1972] and has since become common in the context of coastal ocean dynamics as well [e.g., *Wang and Mooers*, 1976]. Our analyses cover the common data period from May 9, 1983 to November 7, 1983. The Wolf Island sea level is not used because the data are missing for much of this period (Figure 5). Both components of the equatorial currents are used, plus the alongshore component at the coastal moorings. We have multiplied the coastal alongshore currents by −1, so that a poleward geostrophic flow in the southern hemisphere would correspond in sign (phase) to a rise in local sea level. The cross-spectral matrix used as input is comprised of band-averaged spectral estimates with 12 d.f. for the 8.7- to 11.5-day band with a central period of 10 days. This band contains energetic antisymmetric variability along the equator spanning the crossover frequency (Figures 7–10) and strong propagating variability along the coast [*Cornejo-Rodriguez and Enfield*, this issue, Figure 10]. We do not use a wider frequency range because of the rapid variation of zonal phase differences in the equatorial waveguide, within the crossover band.

The first modes of the analyses explain 73% and 61% of the total variances in the data for SLH and currents, respectively. The second modes explain 15% and 23% of the variance. At

TABLE 3. Characteristics of the First Modes of the Separate FDEOFs of Sea Level and Currents

Sea Level Station	rms Amplitude: Band, cm	rms Amplitude: EOF, cm	Explained Variance (EOF, %)	Phase, deg	Speed, m/s
3°N/95°W	0.87	0.68	61	+90	
3°N/85°W	0.55	0.43	63	+79	
2°S/85°W	0.75	0.60	63	−83	
North Isabela	0.42	0.10	5	−36	
Santa Cruz	0.78	0.42	29	+118	
South Isabela	0.55	0.19	11	−26	
Buenaventura	1.79	1.52	72	−12	2.7
Tumaco	1.70	1.45	73	+36	
La Libertad	2.24	2.04	83	−92	
Talara-Paita	1.97	1.86	90	+138	3.0
Callao	1.46	1.10	57	−261	3.1
Current Mooring	**rms Amplitude: Band, cm/s**	**rms Amplitude: EOF, cm/s**	**Explained Variance (FDEOF, %)**	**Phase, deg**	**Speed, m/s**
110°W (u)	2.00	1.14	33	−160	
110°W (v)	3.48	2.39	47	+138	
95°W (u)	1.83	1.19	42	+106	
95°W (v)	3.56	3.29	85	+180	
5°S shelf	3.52	2.61	55	−104	
10°S shelf	2.18	2.01	85	−221	2.3
10°S slope	1.76	1.42	65	−203	2.7

The first modes of the analyses explain 73% and 61% of the total variances, respectively. All sea level phases are referenced to +90° at the 3°N, 95°W IES, and all current phases are referenced to +180° for the meridional velocity at the 0°, 95°W equatorial mooring. Propagation is in the direction of decreasing phase. Poleward propagation speeds are calculated from the phase differences between stations along the coast. Each phase speed is for the indicated station versus the next station equatorward. Station locations are listed in Table 1.

the 95% confidence level the second and higher modes are insignificant by the mode selection rule of *Overland and Preisendorfer* [1982], and we cannot find meaningful interpretations for them.

The statistics for the FDEOF analyses (first modes) are shown in Table 3. The FDEOF phases are referenced to +90° at the 3°N, 95°W IES and to +180° at the 0°, 95°W mooring (meridional velocity) for the SLH and current modes, respectively. These references are chosen a priori to correspond to the expected phase relation for MRG variability at 95°W, which is consistent with the cross-spectral analyses between SLH and meridional velocity (Figure 10). The coherence-squared between the two FDEOFs is 0.90, and the phase between the FDEOFs (using the above references) is 0°. Hence the two FDEOFs are highly coherent, and the phases are related exactly as expected under our a priori assumption. Our convention for phase structures is that propagating signals advance in the direction of decreasing phase.

As expected from their large eigenvalues, the first FDEOF modes reproduce the important features discussed earlier in the individual cross-spectral analyses. Sea levels just north (south) of the equator have phases near +90° (−90°) and the FDEOF amplitudes of meridional currents are almost twice those of the zonal currents along the equator. Phases along the coast decrease poleward into either hemisphere at speeds that are reasonable for coastal trapped waves, and the phases

TABLE 4. Characteristics of the First Mixed FDEOF Mode of Sea Level and Currents

SLH/CM Station	Explained Variance (EOF, %)	Phase, deg	Speed, m/s
95°W (v)	91	+180	
3°N/95°W	61	+85	
3°N/85°W	56	+76	
2°S/85°W	64	−84	
North Isabela	9	−142	
Santa Cruz	35	−115	
South Isabela	13	−32	
Buenaventura	70	−18	2.4
Tumaco	61	+35	
La Libertad	78	−92	
Talara-Paita	95	−141	2.9
5°S shelf	48	−115	
10°S shelf	81	−225	2.5
10°S slope	56	−209	2.9
Callao	64	−261	3.2

The first mixed mode of the analyses explains 59% of the total variability. All phases are referenced to 180° for the meridional velocity at the 95°W equatorial mooring, and propagation is in the direction of decreasing phase. Poleward propagation speeds are calculated from the phase differences between stations along the coast. Each phase speed is for the indicated station versus the next station equatorward. Station locations are listed in Table 1.

of the coastal currents indicate poleward flow when local sea level is high. Zonal phase differences along the equator indicate that fluctuations in SLH and meridional current propagate eastward or westward at high speeds, probably indistinguishable from infinity (i.e., an MRG interpretation). Adding or subtracting 360° from the equatorial phases gives much slower propagation rates, too slow, for example, for lowest mode equatorial Kelvin waves, or in the wrong direction.

The phase speeds along the coast obtained from this analysis are in good agreement with the first-mode, free wave phase speeds calculated by *Brink* [1982] using realistic stratification and bottom topography. Using the phase speeds in Brink's Table 4 for various segments of the Peru coast, we estimate the "theoretical" speeds between Paita and Callao (5°S–12°S) to be 2.6 m/s (versus our observed range of 2.3–3.1 m/s).

Sea level FDEOF amplitudes are generally larger along the coast than at the IESs. *Clarke* [1983], approximating the coast by a vertical meridional wall and assuming that half of the incident MRG energy continues into each hemisphere as coastal Kelvin waves, shows that the equatorial and coastal amplitudes should be comparable but the coastal amplitudes increase poleward in proportion to $|f|^{1/2}$ outside the "corner" region where the two waveguides (equatorial and coastal) overlap. Only Callao (12°S) is far enough poleward for the large-latitude Kelvin wave formula to apply. Assuming that the IES measurements are accurate and represent conditions in the equatorial waveguide unaffected by the boundary, then Clarke's analysis suggests that the amplitude at Callao should be about 2 cm as opposed to the observed amplitude of 1.1 cm. A number of uncertainties arise in making such comparisons, however. First, the coast is not meridional and the equal division of incident energy between hemispheres is unverified. Second, one can speculate that the relevant zonal scale for these very long MRG waves is such that the IESs also lie within a proscribed region where such comparisons are invalid (A. J. Clarke, personal communication, 1987). The fact that the observed FDEOF amplitudes decrease poleward rather than increase is inconsistent with the argument based on energy flux conservation (i.e., the $|f|^{1/2}$ proportionality), but this does not apply in the corner region where the amplitude relationships have not been worked out theoretically.

We have also computed the mixed FDEOF of currents and sea level together by including the cross-spectral estimates between currents and SLH and normalizing all elements of the matrix by the autospectral estimates. In this analysis we have not used the currents at 110°W and include only the meridional currents at 95°W. The results are summarized in Table 4 for the explained variance and phase, showing that the phase relationships are very similar to those of the separate FDEOFs (Table 3). The amplitudes are not shown because of the normalization. Finally, the phases from Table 4 are contoured in Figure 11 to show how the phase varies throughout the region. The three Galapagos stations are excluded from the contour plot, as they badly distort the contours (they are all south of the equator and have large negative values). For plotting purposes, the phase of the meridional curent at 95°W is changed from +180° to 0° because the currents there behave in a manner consistent with MRG behavior, in which the sea level phase changes discontinuously across the equator. The contouring program handles the discontinuity by interpolating to 0° near the equator between the IESs, and this measure allows the contouring to extend westward.

The phases for the first mode are clearly antisymmetric, changing sign from near +90° at stations north of the equator to −90° south of the equator. The zonal orientation of phase lines in the equatorial zone is consistent with a standing (stationary) oscillation, as expected of MRG waves near the crossover frequency. Southward along the Peru coast the phase advances to negative values of larger magnitude, consistent with the conversion of the MRG waves into poleward propagating, coastal trapped Kelvin waves. North of the equator the phase is maximum near Tumaco and then decreases northward to Buenaventura (this is difficult to see in the contours of Figure 11 but is clear in the phases of Table 4).

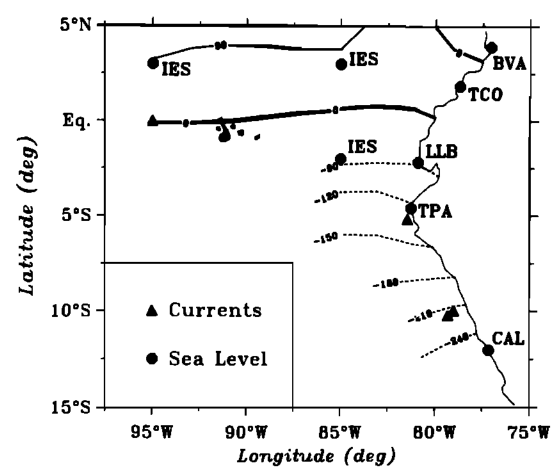

Fig. 11. (Left) Geographic distribution of phase from the first SLH-current mixed-mode FDEOF (from Table 4 as described in the text). Station locations are listed in Table 1. Solid (dashed) contours are for positive (negative) phase.

In summary, the dominant modes of 1- to 2-week variability in the eastern equatorial Pacific sea level and currents are clearly consistent with stationary, antisymmetric oscillations along the equator that transform into poleward propagating trapped waves along the South American coast (both hemispheres). We can find no concrete evidence for the existence of equatorial Kelvin waves in this frequency band, and the remaining (unexplained, higher mode) variability probably consists mostly of unstructured noise.

8. Discussion

The large explained variance of the two FDEOFs and their high mutual coherence indicate a strong coupling of the meridional velocity at 95°W and antisymmetric sea level near the equator with sea level and currents along the coast. The importance of the 95°W meridional velocity together with antisymmetric phase structure across the equator, small phase differences over large zonal distances along the equator, and poleward propagation along the coast are compelling evidence that low wave number MRG waves are the main source of the energetic coastal trapped waves observed during the 1982–1983 El Niño. The spectral analyses, on the other hand, have been especially useful in showing the dominance of MRG waves at 1- to 2-week periods versus Kelvin wave dominance at longer periods. They also demonstrate that the Kelvin and MRG phase relationships agree in that they have the same separation constant as expected for free equatorial waves [*Moore*, 1968; *Gill*, 1982].

It is interesting that the MRG variability dominates so strongly in the 1- to 2-week period band. This can be most readily explained if the waves are forced by large zonal-scale wind oscillations as suggested by *Wunsch and Gill* [1976] and further explained by *Clarke* [1983]. There are selection rules that determine which wave modes are most efficiently excited by a wind field of given zonal extent [*McCreary*, 1984]. In effect, waves with lengths less than twice the extent of the wind field are not as readily excited as longer ones. At periods of 10 days or less, Kelvin waves have wavelengths of less than 2500 km; conversely, MRG waves within the 1- to 2-week band have large phase speeds and wavelengths that range from 3000 km to basin scale.

All of the phase relationships seen in the data sets are consistent with the lowest vertical mode variability of Kelvin and MRG waves. We cannot conclude from this that higher modes are not present, because sea level acts as a filter that blocks higher-mode variability in favor of the lowest mode(s). In fact, the cross spectrum between the meridional currents at 95°W and 110°W (not shown) yields low coherences and nonsensical phases, whereas the SLH-current spectra were quite informative. In the former case, all vertical modes are presumably present, giving a chaotic superposition of phases; in the latter case, the SLH variability has filtered out the higher modes and left only the low-mode phase information. We have no means of analyzing the mooring data for higher vertical modes because the moorings contain only a few current meters with good data return, mainly at depth of 250 m or less.

Perhaps the most intriguing question is, why are the coastal trapped waves so strong during intense ENSO episodes (Figure 6)? The limited analysis we have done on coastal sea level phases across the equator suggests that antisymmetric variability was not strong or present at all before and after the 1982–1983 El Niño. Is it possible that the necessary forcing of MRG waves at low wave numbers is only efficient during ENSO events? If the mode selection argument holds, we need not expect that such wind variability be a narrow-band process near the 10-day period, but only that it be zonally coherent. There is evidence in the meteorological literature that large paired cyclones are a frequent occurrence in the western and west-central Pacific during strong El Niños [e.g., *Keen*, 1982]. The cyclones recur at synoptic intervals and appear to be associated with strong wind fluctuations at equatorial islands [*Luther and Harrison*, 1984]. We have no direct evidence of how the MRG variability is forced, but equatorial winds with zonal coherence scales of 10°–20° longitude or more are a likely candidate. In particular, their interannual variability and dependence on Southern Oscillation conditions should be investigated.

Acknowledgments. Almost inevitably, the thinking process in the development of research is stimulated and guided by conversations with colleagues. Such intellectual contributions to this paper came from contacts with S. P. Hayes, P. Ripa, A. J. Clarke, and J. P. McCreary, to whom we are thankful. We are indebted to M. Wimbush (IESs), S. P. Hayes (pressure gages), and D. Halpern (equatorial moorings) for providing much of our data. The data from tide gages were provided by Instituto Geográfico Agustín Codazzi (Colombia), Instituto Oceanográfico de la Armada (Ecuador), and Dirección de Hidrografía y Navegacion de la Marina (Peru). The research was supported by National Science Foundation grants OCE-8317390, OCE-8315014, and OCE-8709930, and National Oceanic and Atmospheric Administration grants NA85AA-D-CA024 and NA87AA-D-CA082.

References

Allen, J. S., and R. D. Romea, On coastal trapped waves at low latitudes in a stratified ocean, *J. Fluid Mech.*, *98*, 555–585, 1980.

Anderson, M., On the calculation of filter coefficients for maximum entropy spectral analysis, *Geophysics*, *39*, 69–72, 1974.

Brink, K. H., A comparison of long coastal trapped wave theory with observations off Peru, *J. Phys. Oceanogr.*, *12*, 897–913, 1982.

Brink, K. H., J. S. Allen, and R. L. Smith, A study of low frequency fluctuations near the Peru coast, *J. Phys. Oceanogr.*, *8*, 1025–1041, 1978.

Busalacchi, A. J., and J. J. O'Brien, The seasonal variability of a model of the tropical Pacific, *J. Phys. Oceanogr.*, *10*, 1929–1951, 1980.

Busalacchi, A. J., and J. J. O'Brien, Interannual variability of the equatorial Pacific in the 1960s, *J. Geophys. Res.*, *86*, 10,901–10,907, 1981.

Chelton, D. B., P. A. Bernal, and J. A. McGowan, Large-scale interannual physical and biological interaction in the California Current, *J. Mar. Res.*, *40*, 1095–1125, 1982.

Chiswell, S. M., D. R. Watts, and M. Wimbush, Using inverted echosounders to measure dynamic height in the eastern equatorial Pacific during the 1982–1983 El Niño, *Deep Sea Res.*, *33*, 981–991, 1986.

Chiswell, S. M., D. R. Watts, and M. Wimbush, Inverted echo sounder observations of zonal and meridional dynamic height variability in the eastern equatorial Pacific during the 1982–1983 El Niño, *Deep Sea Res.*, *34*, 313–327, 1987.

Clarke, A. J., The reflection of equatorial waves from oceanic boundaries, *J. Phys. Oceanogr.*, *13*, 1193–1207, 1983.

Cornejo-Rodriguez, M. P., and D. B. Enfield, Propagation and forcing of high-frequency sea level variability along the west coast of South America, *J. Geophys. Res.*, this issue.

Eriksen, C. C., M. B. Blumenthal, S. P. Hayes, and P. Ripa, Wind-generated equatorial Kelvin waves observed across the Pacific ocean, *J. Phys. Oceanogr.*, *13*, 1622–1640, 1983.

Gill, A. E., *Atmosphere-Ocean Dynamics*, 662 pp., Academic, Orlando, Fla., 1982.

Keen, R. A., The role of cross-equatorial cyclone pairs in the Southern Oscillation, *Mon. Weather Rev.*, *110*, 1405–1416, 1982.

Knox, R. A., and D. Halpern, Long range Kelvin wave propagation of transport variations in Pacific Ocean equatorial currents, *J. Mar. Res.*, *40*, 329–339, 1982.

Lukas, R., S. P. Hayes and K. Wyrtki, Equatorial sea level response during the 1982–1983 El Niño, *J. Geophys. Res.*, *89*, 10,425–10,430, 1984.

Luther, D. S., Observations of long period waves in the tropical oceans and atmosphere, Ph.D. thesis, 210 pp., Mass. Inst. of Technol., Woods Hole Oceanogr. Inst., Feb. 1980.

Luther, D. S., and D. E. Harrison, Observing long-period fluctuations of surface winds in the tropical Pacific: Initial results from island data, *J. Phys. Oceanogr.*, *14*, 285–302, 1984.

McCreary, J. P., Equatorial beams, *J. Mar. Res.*, *42*, 395–430, 1984.

Moore, D. W., Planetary-gravity waves in an equatorial ocean, Ph.D. thesis, Harvard Univ. Cambridge, Mass., 1968.

Moore, D. W., and S. G. H. Philander, Modelling of the tropical ocean circulation, in *The Sea*, chap. 8, vol. 6, edited by E. D. Goldberg et al., Interscience, New York, 1977.

Overland, J. E., and R. W. Preisendorfer, A significance test for principal components applied to a cyclone climatology, *Mon. Weather Rev.*, *110*, 1–4, 1982.

Quinn, W. H., V. T. Neal, and S. E. Antunez de Mayolo, El Niño occurrences over the past four and a half centuries, *J.Geophys. Res.*, this issue.

Ripa, P., and S. P. Hayes, Evidence for equatorial trapped waves at the Galapagos Islands, *J. Geophys. Res.*, *86*, 6509–6516, 1981.

Romea, R. D., and R. L. Smith, Further evidence for coastal trapped waves along the Peru coast, *J. Phys. Oceanogr.*, *13*, 1341–1356, 1983.

Smith, R. L., Poleward propagating perturbations in currents and sea levels along the Peru coast, *J. Geophys. Res.*, *83*, 379–391, 1978.

Wallace, J. M., Empirical orthogonal representation of time series in the frequency domain, 2, Application to the study of tropical wave disturbances, *J. Appl. Meteorol.*, *11*, 893–900, 1972.

Wallace, J. M., and R. E. Dickenson, Empirical orthogonal representation of time series in the frequency domain, 1, Theoretical considerations, *J. Appl. Meteorol.*, *11*, 887–892, 1972.

Wang, D. P., and C. N. K. Mooers, Long coastal trapped waves off the west coast of the United States, summer 1973, *J. Phys. Oceanogr.*, *6*, 856–864, 1976.

Wunsch, C., and A. E. Gill, Observations of equatorially trapped waves in Pacific sea level variations, *Deep Sea Res.*, *23*, 371–390, 1976.

Wyrtki, K., El Niño: The dynamic response of equatorial Pacific ocean to atmospheric forcing, *J. Phys. Oceanogr.*, *5*, 572–584, 1975.

M. P. Cornejo-Rodriguez, Facultad de Ingenieria Maritima y Ciencias del Mar, Escuela Politecnica del Litoral, Guayaquil, Ecuador.

D. B. Enfield, NOAA Atlantic Oceanographic and Meteorological Laboratory, Miami, FL 33149.

P. A. Newberger and R. L. Smith, College of Oceanography, Oregon State University, Corvallis, OR 97331.

(Received April 23, 1987;
accepted August 22, 1987.)